Journal of Sustainable Mining 17 (2018) 105–110

HOSTED BY

Contents lists available at ScienceDirect

Journal of Sustainable Mining

journal homepage: www.elsevier.com/locate/jsm

Research paper

# Fundamental understanding of diesel-operated man riding vehicle DPM dispersion – A case study

Ramakrishna Morla[a,*], Ajit Godbole[a], Shivakumar Karekal[a], Ram Madhab Bhattacharjee[b], Nasina Balasubrahmanyam[c]

[a] School of Civil, Mining and Environmental Engineering, University of Wollongong, 2522, Australia
[b] Department of Mining Engineering, IIT(ISM), Dhanbad, India
[c] Director General of Mine Safety (DGMS), India

ARTICLE INFO

*Keywords:*
Coal mines
DPM
Diesel-powered man riding vehicle

ABSTRACT

In this paper, an attempt has been made to model DPM flow patterns in the vicinity of man riding vehicle(s) operating in a coal mine environment. The DPM flow patterns are modelled using the techniques of computational fluid dynamics (CFD) and validated using field experimental measurements. The models show that if the vehicle is stationary, DPM particles are dispersed towards the center of gallery. Beyond 20 m downstream of the vehicle, the DPM particles occupy the entire cross-section of the roadway. If movement of the vehicle is considered, the miners may be exposed to a high concentration of DPM due to the engines running at full capacity and the resultant air flow induced by the movement of the vehicle.

## 1. Introduction

A number of coal mines operate in multi-seams comprising a large number of working sections separated by long distances. Man-riding vehicles are used to minimize the miners' travel time between working sections and thus improve their performance. Several underground coal mines use man riding vehicles in which diesel is used as the fuel.

As underground coal mines go ever deeper and spread over larger areas in an attempt to meet ever-increasing production targets, there is a correspondingly significant increase in the usage of diesel-powered man riding vehicles. This is because these vehicles offer greater flexibility to travel longer distances and between working sections of a coal mine. The use of these vehicles is efficient, as evidenced by ease of maintenance, consistency and durability. Many nations have depended on these vehicles because of these reasons (AIOH, 2013). The main problem with these vehicles are their exhaust gases, which contain a mixture of diesel particulate matter (DPM) and other pollutant gases such as Nitrogen Oxides (NOx), Hydrocarbons (HC) and Carbon Monoxide (CO) (MDG 29, 2008).

DPM is the by-product of incomplete combustion of diesel fuel in the diesel engine. It is made up primarily of carbon, ash, abrasive metallic particles, sulphates and silicates. The effective density (mass per unit volume) of DPM decreases sharply from 1.2 g/cm$^3$ for 30 nm particles to 0.3 g/cm$^3$ for 300 nm particles (Bugarski, Janisko, Cauda, Noll, & Mischler, 2012). The effective density of agglomerated diesel particles varies from 1.1 to 1.2 g/cm$^3$. The chemical composition of DPM has not been observed to follow any trend and it mainly depends on engine oil and diesel chemical composition (Bartlett et al., 1992).

The size of DPM particles varies from 5 nm to 10,000 nm. About 90% of particles are under 30 nm size (David, 2002). DPM particle deposition in the human respiratory tract mainly depends on the size of the particles. The diesel aerosol particles of size ranging from 3 nm to 500 nm readily penetrate the alveolar regions where gas exchange occurs. The removal of solid diesel aerosols from unciliated alveolar regions is substantially slower than that of aerosols deposited in the ciliated upper lung region. On average, 30% ± 9% of the total number of diesel aerosols with a median diameter of 125 nm and a geometric standard deviation of 1.7 get deposited in the human respiratory tract (Bugarski et al., 2012).

Various research studies have been conducted to better understand the effects of DPM on human health, for example AIOH (2013), Morla and Karekal (2017) and Attfield et al. (2012). These studies have concluded that exposure to diesel exhaust may cause cancer in humans.

As per coal mines regulations, the recommended 8-h time weighted average exposure standard of elemental carbon (EC) fraction when expelled from a diesel engine is 0.1 mg/m$^3$. Which is approximately equal to 0.16 mg/m$^3$ total carbon (TC) or 0.2 mg/m$^3$ diesel particulates (DP). The minimum ventilation quantity required to overcome diesel

* Corresponding author.
*E-mail address:* rm746@uowmail.edu.au (R. Morla).

https://doi.org/10.1016/j.jsm.2018.04.004
Received 8 January 2018; Received in revised form 20 March 2018; Accepted 25 April 2018
Available online 26 April 2018

emissions and heat stress where a diesel engine operates shall be such that ventilation current of not less than 0.06 $m^3$/s/kW of maximum capacity of the engine or 3.5 $m^3$/s whichever is greater. If more than one diesel engine is being operated in the same ventilation current the diesel engine rated kW shell be added (MDG 29, 2008). However, the statutory ventilation quantities may not be possible to send in all working conditions. This is an urgent concern, because DPM is known to be a carcinogenic agent that can have a serious adverse effect on the miners' health after prolonged exposure.

To regulate the DPM exposure to the miner and to design control strategies, an effective mapping of DPM near diesel-powered vehicles in operation is required. This paper outlines a study of DPM flow patterns near a diesel-powered man riding vehicle, using CFD simulations that are validated against field experimental data. Field experiments have been conducted in two stages using an Airtec real time DPM monitoring instrument. In stage one, DPM concentration was monitored near a stationary vehicle and in stage two DPM concentration monitored in the vicinity of a moving vehicle.

## 2. Material and methods

### 2.1. Details of the experimental mine

Field experiments were conducted in one of the Indian coal mines, mine A (not named due to confidentiality issues). The field experiments were carried out in one of the eight working seams in the mine. The gradient of the experimental seam varies from 1 in 16 to 1 in 22 and the "gassiness" of the seam is considered as a degree one. The depths of working sections range from 50 m to 400 m. The mine has two "depillaring" panels with continuous miners, one longwall panel and a few development sections. The overall production of the mine is 3.5 million tonnes with 3100 manpower.

The mine has five intake airways and two return air shafts, the ventilation system of the mine is operated by two axial flow fans. Fan A generates an air flow of 150 $m^3$/s at 510 Pa pressure and fan B generates air flow of 140 $m^3$/s at 400 Pa pressure. The distance between the pit bottom to the working section is about 4 km. The mine operators use three diesel-powered man riding vehicles to travel this distance. Fig. 1a shows a typical diesel-powered man riding vehicle used in the mine. The vehicle can carry 16 passengers and maximum speed of the vehicle is 25 km/h.

### 2.2. Details of the field experiment

An Airtec real time DPM monitoring instrument was used for the field experiment. Fig. 1b show the details of the DPM monitor. This instrument is a compact and highly portable real-time elemental carbon (EC)/DPM monitor. This instrument works on the principle of real time particle capture and light transmission method to yield EC values, which closely correlates with NOISH 5040 measurements of EC (Khan, 2017).

During stage one field experiments, three sampling stations located at 1 m, 5 m and 10 m from the vehicle were selected. Each station had three sampling points at a height of 1.2 m from the floor. During the experiment, the flow rate of the instrument was adjusted to $2.83 \cdot 10^{-5}$ $m^3$/s (1.7 L per minute). Fig. 2 shows the locations and arrangements of sampling stations and sampling points (a, b and c) located at the rear of the man riding vehicle. During this experiment, the engine was run under a "no-load" condition.

Stage one experiment was conducted in an isolated intake galley of the mine. The average width and height of the mine gallery are 6 m and 2.7 m respectively, as measured with a laser-powered distance measuring instrument. Air velocity was monitored with a vane anemometer and cross-checked against spot measurements with a digital anemometer. During the experiment, the average velocity of the air flow was 1.26 m/s. To eliminate intake air DPM concentration, the experiment was conducted in one of the main intake which passes from surface to the mine working section. The velocity of the DPM-carrying smoke was measured with a digital anemometer and was found to be 54 m/s. The temperature of the exhaust smoke was measured with thermocouple digital thermometer, and was found to be 323 K.

### 2.3. CFD modelling

The basic DPM related CFD modelling studies have been conducted in metal/no-metal mines using 30 kW stir skid loader (Zheng, Lan, Magesh, & Tien, 2011; Zheng, Lan, Thiruvengadam, & Tien, 2011, Zheng, Thiruvengadam, Lan, & Tien, 2015a, 2015b). In this paper, DPM simulation studies conducted with man-riding vehicle in a coal mine using commercially available CFD package ANSYS Fluent (version 18.2). CFD simulations were carried in the following four steps.

#### 2.3.1. Construction of computational domain

A 50-m long ventilation gallery was designed for simulations, width and height of the gallery were 6 m and 2.7 m. Man riding vehicle was designed and imported from the 3D CAD modelling. Length, width and height of the man riding were 6.25 m, 2 m, 1.95 m respectively. The location of the smoke pipe is behind the left front wheel and opposite side to the vehicle operator. The engine was equipped with diesel particulate filter and the exhaust flow is a mixture of DPM and air. Dip of the air way was considered as 1 in 22. Fig. 3 shows the details of the constructed CFD model.

#### 2.3.2. Construction of computational mesh

Fig. 4 shows the details of meshed man riding vehicle (a) and man riding vehicle with gallery (b). To achieve accurate results, finer mesh was used with half-million computational cells. The minimum size of the cells was $7.3 \cdot 10^{-3}$ m, minimum edge length of cells was 0.025 m and size function was proximity and curvature. Program controlled inflation with seven layers were used for the mesh.

#### 2.3.3. Setting up the flow conditions

Intake air was supplied through the inlet of the galley with 1.26 m/s velocity and 300 K temperature. DPM was released from the smoke pipe

a. Diesel-powered man riding vehicle b. DPM monitor

**Fig. 1.** Diesel-powered man riding vehicle and DPM monitor.

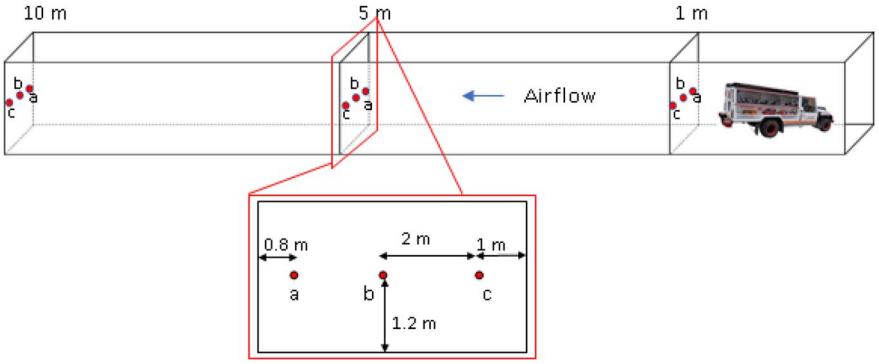


**Fig. 2.** Locations of sampling stations and sampling points with respect to DPM source.

with a velocity of 54 m/s and temperature of 323 K. For this investigation, DPM is treated as a gas and chemical reactions were not considered. The flow in the domain was considered as Boussinesq approximation and turbulent.

### 2.3.4. Governing equations

To model turbulence, Reynolds-Averaged Navier-Stokes equation was used. In Reynold's averaging, the solution variables in the exact Navier-Stokes equations are consisting of time averaged and fluctuated components for velocity components (ANSYS, 2013).

$$u_i = \overline{u_i} + u_i' \tag{1}$$

where $\bar{u}_i$ and $u_i'$ are mean and fluctuating velocity components ($i = 1, 2, 3$).

Reynolds-averaged Navier-Stokes (RANS) equation was obtained by substituting time and average velocity in momentum equation:

$$\frac{\partial \rho}{\partial t} + \frac{\partial}{\partial x_i}(\rho u_i) = 0 \tag{2}$$

$$\frac{\partial}{\partial x}(\rho u_i) + \frac{\partial}{\partial x_j}(\rho u_i u_j) = -\frac{\partial p}{\partial x_i} + \frac{\partial}{\partial x_j}\left[\mu\left(\frac{\partial u_i}{\partial x_j} + \frac{\partial u_j}{\partial x_i} - \frac{2}{3}\delta_{ij}\frac{\partial u_l}{\partial x_l}\right)\right] + \frac{\partial}{\partial x_j}(-\rho\,\overline{u_i' u_j'}) \tag{3}$$

where $-\rho\,\overline{u_i' u_j'}$ is Reynolds stress and can be solved with Boussinesq hypothesis and Reynolds stress models (RSM). In Boussinesq hypothesis, the Reynolds stress is related to the mean velocity gradient (ANSYS, 2013):

$$-\rho\,\overline{u_i' u_j'} = \mu_t\left(\frac{\partial u_i}{\partial x_j} + \frac{\partial u_j}{\partial x_i}\right) - \frac{2}{3}\left(\rho k + \mu_t \frac{\partial u_k}{\partial x_k}\right)\delta_{ij} \tag{4}$$

To determine turbulent viscosity $\mu_t$, the $k$-$\varepsilon$ model was used.

$$\mu_t = \rho C_\mu \frac{k^2}{\varepsilon} \tag{5}$$

where $C_\mu$ is a constant, $k$ is the turbulence kinetic energy and $\varepsilon$ is the dissipation rate of $k$. Turbulent heat transport is modelled using the concept of the Reynolds analogy to turbulent momentum transfer. The modelled energy equation is as follows:

$$\frac{\partial}{\partial t}(\rho E) + \frac{\partial}{\partial x_i}[u_i(\rho E + p)] = \frac{\partial}{\partial x_j}\left[\left(k + \frac{c_p \mu_t}{\sigma_k}\right)\frac{\partial T}{\partial x_j} + u_i(\tau_{ij})_{eff}\right] + S_h \tag{6}$$

where $k$ is the thermal conductivity, $E$ is the total energy and $(\tau_{ij})_{eff}$ is the deviatoric stress tensor, defined as

$$(\tau_{ij})_{eff} = \mu_{eff}\left(\frac{\partial u_j}{\partial x_i} + \frac{\partial u_i}{\partial x_j}\right) - \frac{2}{3}\mu_{eff}\frac{\partial u_k}{\partial x_k}\delta_{ij} \tag{7}$$

The standard $k$-$\varepsilon$ model is based on the model transport equations $k$ and $\varepsilon$. The model transport equation for $k$ is derived from the exact equation, while the model transport equation for $\varepsilon$ was obtained using physical reasoning and bears little resemblance to its mathematically exact counterpart.

In the derivation of the $k$-$\varepsilon$ model, the assumption is that the flow is fully turbulent, and the effect of molecular viscosity is negligible. As the mine air is considered as fully turbulent flow, the $k$-$\varepsilon$ model is valid for mine air.

The turbulent kinetic energy, $k$, and its rate of dissipation, $\varepsilon$, are

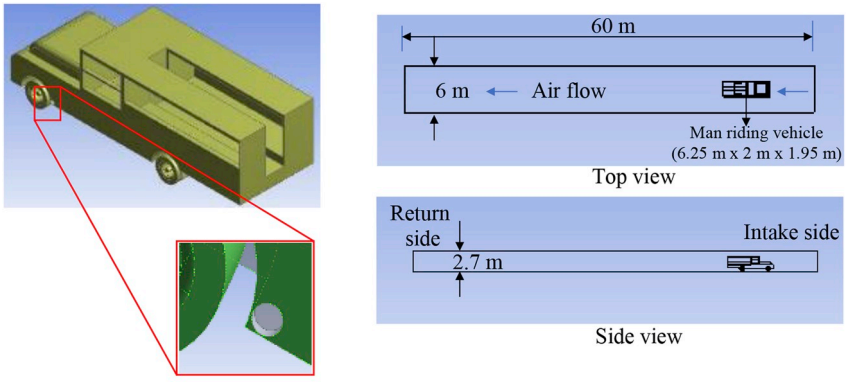


a. CFD model of man-riding vehicle with detail showing location of exhaust port

b. CFD model of man-riding vehicle with gallery

**Fig. 3.** CFD model of man riding vehicle and experimental gallery.

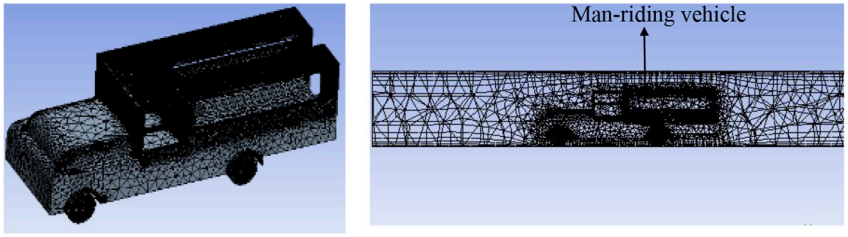


**Fig. 4.** Mesh model of man riding vehicle and experimental gallery.

**Table 1**
Comparison of simulated results with experimental results.

| Sampling point | At 1 m sample station | | | At 5 m sample station | | |
|---|---|---|---|---|---|---|
| | Experimental value (μg/m$^3$) | Simulation value (μg/m$^3$) | Difference % | Experimental value (μg/m$^3$) | Simulation value (μg/m$^3$) | Difference % |
| a | 185.8 | 176 | −5.2 | 149.0 | 130 | −12.7 |
| b | 50 | 46 | −8.0 | 117 | 110 | −5.9 |
| c | 0 | 0 | 0 | 16 | 16 | 0 |
| | At sample station 10 m | | | | | |
| a | 127.4 | 130 | 2.0 | | | |
| b | 116.6 | 100 | −14.2 | | | |
| c | 50.0 | 57 | 14.0 | | | |

Note: difference in % is the difference between simulation results and test results and is calculated as (simulation value – Experimental value)/experimental value) × 100%.

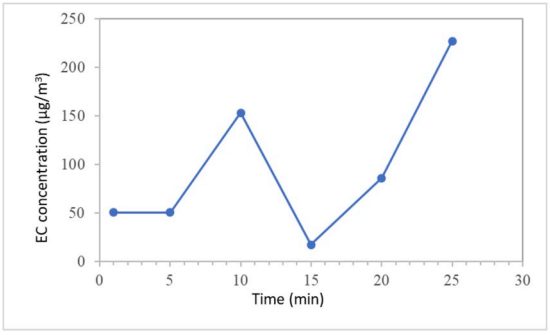


**Fig. 5.** EC concentration at passenger seat (moving vehicle).

obtained from the following governing equations (ANSYS, 2013):

$$\frac{\partial}{\partial t}(\rho k) + \frac{\partial}{\partial x_i}(\rho k u_i) = \frac{\partial}{\partial x_j}\left[\left(\mu + \frac{\mu_t}{\sigma_k}\right)\frac{\partial k}{\partial x_j}\right] + G_k + G_b - \rho\varepsilon - Y_M + S_k \tag{8}$$

$$\frac{\partial}{\partial t}(\rho\varepsilon) + \frac{\partial}{\partial x_i}(\rho\varepsilon u_i) = \frac{\partial}{\partial x_j}\left[\left(\mu + \frac{\mu_t}{\sigma_\varepsilon}\right)\frac{\partial \varepsilon}{\partial x_j}\right] + C_{1\varepsilon}\frac{\varepsilon}{K}(G_k + C_{3\varepsilon}G_b) - C_{2\varepsilon}\rho\frac{\varepsilon^2}{K} + S_\varepsilon \tag{9}$$

where $G_b$ is the generation of turbulent kinetic energy due to buoyancy, $G_k$ is the production of turbulent kinetic energy due to the mean velocity gradient.

To conduct DPM investigations in a mine gallery, a "species transport model" was used. ANSYS fluent predicts the local mass fraction of each species, $Y_i$, though the solution of a convection-diffusion equation for the $i$th species. The conservation equation takes the following general form:

$$\frac{\partial}{\partial t}(\rho Y_i) + \Delta(\rho\vec{v}Y_i) = -\Delta\vec{J_i} + R_i + S_i \tag{10}$$

## 3. Results and discussions

### 3.1. Results and discussions of the field experiments

Table 1 shows the stage one field monitored EC concentration

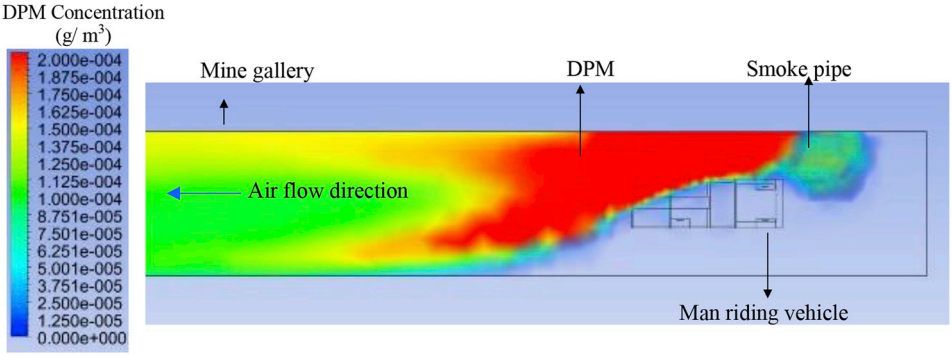


**Fig. 6.** DPM flow pattern – top view.

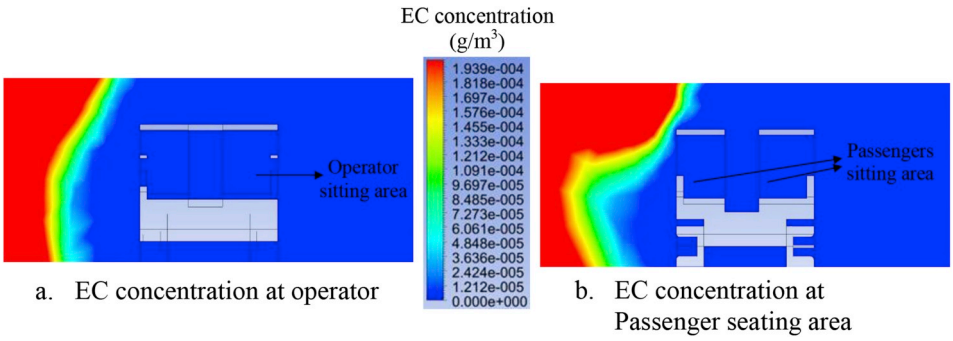


**Fig. 7.** EC concentration at operator and passenger seating area.

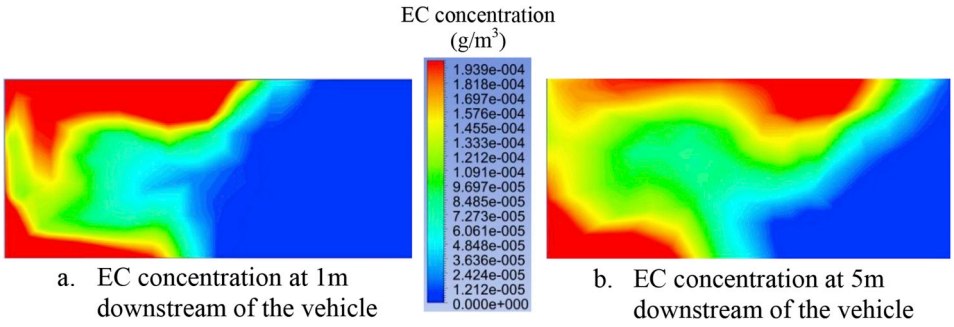


**Fig. 8.** EC concentration at 1 m and 5 m downstream of the vehicle.

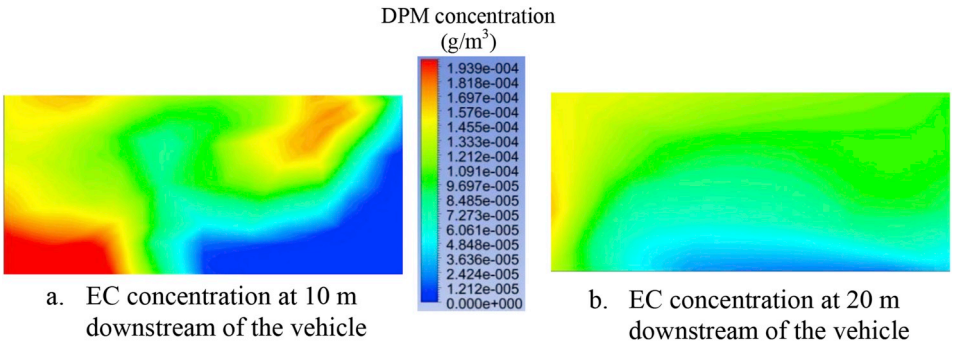


**Fig. 9.** EC concentration at 10 m and 20 m downstream of the vehicle.

results at the three sampling stations. From the table, it can be observed that at 1 m downstream side, high EC concentration is at sample point "a". At sample point "b" and "c", EC concentration gradually increased from 1 m to 10 m downstream side of the vehicle.

In the second stage of the field experiment, EC concentration was measured in the passenger seat during vehicle movement. In this stage, vehicle was run in full capacity and engine emitted maximum size of flumes. EC measurements were taken during the vehicle was travelled from the pit bottom to the continuous miner district of 4 km distance. Maximum speed of the vehicle on level ground is 25 km/h and on 1 in 7 gradient road is 18 km/h. During the experiment, the vehicle was travelled at an average speed of 10 km/h (2.7 m/s) and air velocity in the road was varied from 1 m/s to 2.5 m/s. Fig. 5 shows the EC concentration at different time periods during 4 km travel distance. The concentration changes with relative velocities between vehicle and air.

### 3.2. Results and discussions of the CFD modelling

Fig. 6 shows the results of CFD simulations from top view. From the figure, it can be observed that high DPM concentration is in between the smoke pipe side of the vehicle and wall. At the downstream side of the vehicle, DPM particles spread whole gallery.

Fig. 7 shows the DPM concentration at operator and at the passenger sitting area. At operator's location, Fig. 7a, high DPM concentration is observed near wall and no DPM concentration is observed near operator. At passenger sitting area (4 m downstream to the smoke pipe), Fig. 7b, high DPM concentration is between vehicle and wall and no concentration is observed near passenger sitting location.

Fig. 8 shows the DPM concentration at 1 m and 5 m downstream to the vehicle. At 1 m downstream to the vehicle, Fig. 8a, maximum concertation is near left side of the roof, trace of concentration was observed roadway, and negligible concentration was observed at the right side of the road way. At 5 m downstream to the vehicle, Fig. 8b, DPM flow moved towards the right side of the roadway maximum DPM concentration is near the roof of the roadway center.

At 10 m downstream side of the vehicle, Fig. 9a, EC concentration at the center of the road way is 150 $\mu g/m^3$ and low concentration is observed at the right side of the road way. At 20 m downstream to the vehicle, Fig. 9b, EC particles spread entire road way. EC concentration at the center of the road way is reduced to 110 $\mu g/m^3$.

### 3.3. Model validation

Table 1 shows the compared results of base case simulations and

field experiments at 1 m, 5 m and 10 m downstream of the vehicle and at the sample point a, b and c. The simulated results were in fair agreement with the measured data at a number of instances and such results which slightly deviated from the measured data can be due uneven gallery walls surface were not considered while modelling. The difference varies from −14.2% to +14%.

## 4. Conclusions

In this study, field measurements and CFD investigations were used to map contours of DPM particle flow of a man riding vehicle. CFD models were validated with the field experimental data. The simulated results were well in agreement with the measured data. The studies showed that if the vehicle is stationary, high DPM concentration is between the smoke pipe side of the vehicle and the wall. At the vehicle downstream side, DPM flow moves towards the center of the gallery. At 20 m from the vehicle, DPM particles spread throughout the entire roadway. The investigations also concluded that miner's may also expose to high concentration of EC up to 226.8 μg/m$^3$ during travelling in the vehicle, this concentration varies with resultant velocities between vehicle and air.

## Ethical statement

None.

## Funding body

None.

## Conflict of interest

Authors state that there is not any conflict of interest.

## Acknowledgements

The authors sincerely thank M/s Coal India Limited, DGMS, Govt. of India and IIT (ISM) Dhanbad for providing necessary resources and extending cooperation during the field experiments.

## Appendix A. Supplementary data

Supplementary data related to this article can be found at https://doi.org/10.1016/j.jsm.2018.04.004.

## References

AIOH. (2013). *Diesel particulate matter & occupational health issues.* Position Paper. Prepared by AIOH Exposure Standards Committee. Retrieved October 15, 2017, from https://www.aioh.org.au/documents/item/15.

ANSYS. (2013). *ANSYS fluent theory guide.* Canonsburg, PA: ANSYS, Inc.

Attfield, M. D., Schleiff, P. L., Lubin, J. H., Blair, A., Stewart, P. A., Vermeulen, R., et al. (2012). The diesel exhaust in miners study: A cohort mortality study with emphasis on lung cancer. *Journal of the National Cancer Institute, 104*(11), 869–883. https://doi.org/10.1093/jnci/djs035.

Bartlett, C. J. S., Betts, W. E., Booth, M., Giavazzi, F., Guttmann, H., Heinze, P., et al. (1992). *The chemical composition of diesel particulate emissions*. Report no. 92/51, Retrieved October 27, 2017, fromhttps://www.concawe.eu/wp-content/uploads/2017/01/rpt_92-51ocr-2004-01337-01-e.pdf.

Bugarski, A. D., Janisko, S. J., Cauda, E. G., Noll, J. D., & Mischler, S. E. (2012). *Controlling exposure to Diesel emissions in underground mines.* Englewood, CO: Society for Mining, Metallurgy, and Exploration, Inc. (SME).

David, B. K. (2002). *Measurement of engine exhausts particle size.* Presented at University of California. 17 February 2000. Retrieved November 21, 2017, from http://www.me.umn.edu/centers/mel/reports/dbkucdavis.pdf.

Khan, U. M. (2017). *Real-time diesel particulate matter monitoring in underground mine atmospheres, association with the standard method and related challenges.* Doctoral Dissertation Missouri University of Science and Technology. Retrieved November 1, 2017, from http://scholarsmine.mst.edu/doctoral_dissertations/2625/.

MDG 29 (Mine Design Guideline 29). (2008). *Guideline for the management of diesel engine pollutants in underground environments. Produced by Mine Safety Operations Division.* New South Wales Department of Primary Industries. Retrieved January 5, 2018, from http://www.resourcesandenergy.nsw.gov.au/_data/assets/pdf_file/0011/419465/MDG-29.pdf.

Morla, R., & Karekal, S. (2017). Diesel particulate matter investigations in underground coal mines. *International Journal of Engineering and Technology, 9*(4), 2698–2703. https://doi.org/10.21817/ijet/2017/v9i4/170904401.

Zheng, Y. (2011). *Diesel particulate matter dispersion analysis in underground metal/non-metal mines using CFD.* Ph.D. thesis Missouri University of Science and Technology. Retrieved December 11, 2017 from https://scholarsmine.mst.edu/cgi/viewcontent.cgi?article=3018&context=doctoral_dissertations.

Zheng, Y., Lan, H., Thiruvengadam, M., & Tien, J. C. (2011). DPM dispersion experiment at MST's experimental mine and comparison with CFD simulation. *Journal of Coal Science and Engineering, 17*(3), 285–289. https://doi.org/10.1007/s12404-011-0311-1.

Zheng, Y., Thiruvengadam, M., Lan, H., & Tien, C. J. (2015a). Effect of auxiliary ventilations on diesel particulate matter dispersion inside a dead-end entry. *International Journal of Mining Science and Technology, 25*(6), 927–932. https://doi.org/10.1016/j.ijmst.2015.09.008.

Zheng, Y., Thiruvengadam, M., Lan, H., & Tien, C. J. (2015b). Simulation of DPM distribution in a long single entry with buoyancy effect. *International Journal of Mining Science and Technology, 25*(1), 47–52. https://doi.org/10.1016/j.ijmst.2014.11.004.